ORIGINAL ARTICLE

Veterinary Research Forum. 2021; 12 (2) 167 – 173
doi: 10.30466/vrf.2019.98930.2361
Journal Homepage: vrf.iranjournals.ir

Veterinary Research Forum

Conventional histomorphometry and fast free of acrylamide clearing tissue (FACT) visualization of sciatic nerve in chicken (*Gallus domesticus*)

Abdolrasoul Malekpour[1,2], Farhad Rahmanifar[3]*

[1] DVM Graduate, School of Veterinary Medicine, Shiraz University, Shiraz, Iran; [2] Legal Medicine Research Center, Legal Medicine Organization, Tehran, Iran; [3] Department of Basic Sciences, School of Veterinary Medicine, Shiraz University, Shiraz, Iran.

Article Info

Article history:

Received: 03 December 2018
Accepted: 17 April 2019
Available online: 15 June 2021

Keywords:

3D imaging
Chicken
FACT
Histomorphometric study
Sciatic nerve

Abstract

Histomorphometry and use of the fast free of acrylamide clearing tissue (FACT) protocol were studied on the sciatic nerve in chicken (*Gallus domesticus*). In the first part of the study, the sciatic nerves of 20 chickens of four age groups (7, 14, 26 and 40 days) were studied (n=5 birds per age class). Their sciatic nerve samples were stained with Hematoxylin and Eosin and Masson's trichrome and were histomorphometrically evaluated. In the second part of the study, FACT protocol was applied on the sciatic nerve of a 26 days old chicken. After clearing of 1.00 mm-thick sciatic nerve sections, they were immunolabelled using Hoechst for nuclei staining and recorded by a Z-stack motorized fluorescent microscope. In the conventional histomorphometry, the epineurium, perineurium and endoneurium were thicker and the nerve bundle diameter was bigger in the left sciatic nerve of chicken of all age groups compared to the right sciatic nerve. On the contrary, the axon diameter and the myelinated nerve fiber diameter were bigger, the myelin sheath was thicker, the nodes of Ranvier intervals were higher and the density of myelinated nerve fibers was also higher in the right sciatic nerve compared to the left one. In conclusion, histomorphometric parameters in the left and right sciatic nerve during chicken growth were significantly different. Furthermore, the FACT protocol could be used for the 3D imaging of the chicken sciatic nerve and its immunostained evaluation.

Introduction

Three-dimensional (3D) imaging of the nervous system has been recently developed to study cellular and extracellular markers in the tissue.[1,2] However, it requires transparency of the tissue in order to enable the light to penetrate and detect immunolabelled molecules. The phospholipids of the cellular membrane are scattering light in cells, therefor, removal of lipids is necessary to achieve tissues transparency. Several procedures have been developed to process the tissue and convert it into transparent material including methods for the lipid removal those have been developed recently. Furthermore, several techniques have been introduced for 3D imaging of the nervous system such as CLARITY,[3] passive CLARITY,[2] PACT,[4] PARS,[4] SWITCH,[5] FASTClear,[6] and FACT.[7]

Sciatic nerve (nervus ischiadicus) is the largest and the longest nerve in the body. The nerve is used as a model for the morphometric study of myelinated and non-myelinated peripheral nerve components. So far, studies on the peripheral nerve in the Wistar rats[8,9] and the rabbit[10] have been conducted.

Ronchi *et al.* and Barreiros *et al.* also used light microscopy for quantitative assessment of normal and regenerated peripheral nerve fibers and morphometric analyses of crushed sciatic nerves.[11,12] Kemp *et al.* observed that myelinated nerve fibers were compromised by the normal ageing process, whereas un-myelinated nerve fibers seemed to remain unaltered or, at least, less affected.[13]

Ikeda and Oka analyzed the relationship between motor nerve conduction velocity and morphological changes in regenerating nerve fibers at different times after sciatic nerve transection.[14] Understanding the growth pattern of sciatic nerve in details may help us in the treatment of the sciatic nerve and other peripheral nerve related anomalies and diseases.

***Correspondence:**

Farhad Rahmanifar. DVM, PhD
Department of Basic Sciences, School of Veterinary Medicine, Shiraz University, Shiraz, Iran
E-mail: rahmanifar@shirazu.ac.ir

Histomorphometric studies have not been conducted on sciatic nerve of the chicken of different ages, yet. Therefore, our aim was to evaluate histomorphometric parameters of the left and right sciatic nerves in chicken of different ages. Furthermore, we introduced FACT protocol for 3D imaging of chicken sciatic nerve.

Materials and Methods

Birds. All experimental procedures on the broiler chickens (*Gallus domesticus*) were performed according to the instructions of the Animal Care Committee of the Shiraz University (No. tez1295, Date: 14/7/2012).

Histomorphometry of the sciatic nerve. Twenty chickens were euthanized and the sciatic nerves dissected. Almost equal sized samples (0.50-1.00 cm) were isolated from the left and the right sciatic nerves and placed in a container containing fixative solution (10.00% buffered formalin to 20 times the sample volume). After 24 hr the formalin-fixed tissue blocks trimmed down and placed in the fixative. The samples were stabilized in a tissue chamber to the take out the tissue fixative solution, and they were put in the container containing distilled water (2500A; Autotechnicon, Lipshaw, USA). Overall, the Auto-technicon machine consisted of 12 canisters containing different solutions in which the dehydration process and paraffin embedding of the tissue were done, automatically. After 24 hr the device was removed and tissue samples were prepared for molding. The samples were molded in lead blocks by liquid paraffin. Molded samples were cut with a microtome. All samples were cut to 5.00 µm thickness slices both transversely and longitudinally. The paraffin sections were affixed to a glass slide with an adhesive made from egg whites and glycerin. The prepared slides were numbered and returned to the oven for 1 hr at 56.00 ˚C while drying and additional paraffin sections and slides were melt. All slides of each sample were archived for staining. Ten slides of each sample were stained with Hematoxylin and Eosin[15] and green Masson's trichrome.[16] Stained sections were studied using quantitative histomorphometric method. In this method, the slides were evaluated under a light microscope and the diameters of the nerve bundle, perineurium, endoneurium, nerve fiber, and axon, the thicknesses of epineurium and myelin, the distance between the node of Ranvier, and the number of axon in the millimeter square of the tissue transverse section were measured (Fig. 1).

FACT protocol and immunolabelling of the nuclei. A 26-day-old chicken was euthanized and right and left sciatic nerves were harvested. Samples were put in 4.00% paraformaldehyde (PFA) diluted in phosphate-buffered saline (PBS) solution (0.10 M) as a fixative solution (pH 7.50) and were fixed at 4.00 ˚C for 3 days.[17] Furthermore, the whole sciatic nerves were cleared with 8.00% (w/v) sodium dodecyl sulfate (SDS; Sigma-Aldrich, St. Louis, USA) in 0.10 M PBS (pH 7.50) that was supplemented with 0.02% sodium azide (Sigma-Aldrich), at 37.00 ˚C with mild rotational horizontal shaking (100 rpm). The solutions were refreshed daily for three days, then weekly until visual confirmation of the transparency was achieved by viewing black grid lines on a white sheet of paper through the tissue samples.

After processing the sciatic nerves according to the FACT protocol,[7] the SDS was removed by washing in PBS and sodium azide for 24 hr in mild rotational shaking. For saving antibody consumption, 1.00 mm sections were performed. The sciatic nerve sections were incubated in Hoechst 33342 (Sigma-Aldrich) diluted in PBS and sodium azide (1:200) in a shaker incubator at 37.00 ˚C for 12 hr.

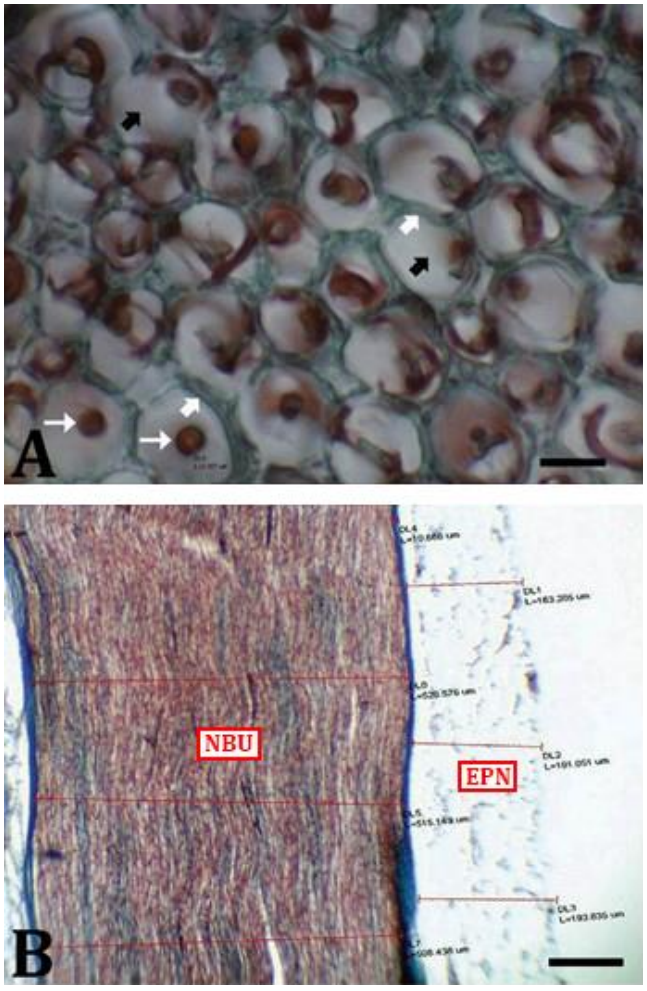

Fig. 1. Histomicrograph of sciatic nerves at the various ages of chicken. **A)** Axon (white narrow arrows), myelin sheath (black thick arrows) and endoneurium (white thick arrows) of 14 days old chicken (Masson's trichrome staining, Scale bar = 5.00 µm); **B)** Epineurium (EPN) and nerve bundle (NBU) of left sciatic nerve of 26 days old chicken (Masson's trichrome staining, Scale bar = 100 µm).

Furthermore, the pieces were washed twice in PBS and sodium azide, and were gently shaken in the same washing solution for 12 hr at 37.00 ˚C in an aluminum foil-covered tube. For refractive index matching, the pieces were placed in 80.00% glycerol for 12 hr at the room temperature prior to the imaging.

3D fluorescent microscopy and image preparation. For 3D imaging the sciatic nerve samples were individually mounted between two glass slides and using a non-colorful putty which was pasted between slides and around the tissue such a horse-shoe chamber (1.00 - 2.00 mm thickness), the tissue was supported between two glasses. The chamber between the two slides was filled with fresh 80.00% glycerol. The mounted sciatic nerve samples were recorded layer by layer with a microscope (U-LH100HGAPO; Olympus, Tokyo, Japan), camera (DP73; Olympus), and cellSens imaging software (version 1.12; Olympus). For this purpose, the selected area was automatically recorded by the Z-stack option of motorized stage each 10.00 µm and for thickness of 150 to 200 µm from tissue surface. After the images were recorded, the TIFF image sequences were transferred to Imaris software (version 7.4.2; Bitplane AG; Zürich, Switzerland) for 3D reconstruction. Because of the large amount of data, a workstation server was used for the image 3D reconstructions.

Statistical analysis. After collecting the results, the mean and standard deviations were analyzed by one-way ANOVA (for comparison of morphometric data between age groups) or *t*-test (for comparison of data between right and left sciatic nerves) using SPSS software (version 19.0; IBM Corp., Armonk, USA). A p value less than 0.05 was considered as a significant difference.

Results

Table 1 shows the average histomorphometric parameters of the left and the right sciatic nerve in different age categories of chicken. The minimum and maximum thicknesses of the epineurium in the both right and left sciatic nerves were at the same age of seven days and 26 days, respectively. A slight increasing in the thickness of both sides was observed until the age of 26 days. However, at the age of 40 days the epineurium thickness was lesser than at the age of 26 days.

The minimum perineurium thickness was in the right sciatic nerve at the age of seven days and in the left at the age of 26 days. The maximum perineurium thickness was observed at the age of 40 days in both the right and left sciatic nerves. The perineurium diameter of the right sciatic nerve was increased while the chicken grows. However, the perineurium diameter of the left sciatic nerve was decreased gradually until the age of 26 days and then reached to the maximum diameter at the age of 40 days.

The endoneurium thickness in the right sciatic nerve did not change significantly during chicken growth. The minimum endoneurium thickness of the left sciatic nerve was at the age of seven days. The endoneurium diameter of the left sciatic nerve was increasing with age, however, it reached its maximum in the left sciatic nerve at the age of 14 and 40 days.

The nerve bundle minimum diameter of the right and left sciatic nerve was at the age of seven days and the maximum at the age of 40 days. A gradual increase of the nerve bundle diameter was observed in the left and right sciatic nerve.

Table 1. Histomorphometric parameters (mean ± SD) of left and right sciatic nerves at different ages of chicken.

Parameters	Sciatic nerve	Days			
		7	14	26	40
Epineurium thickness (µm)	Right	42.80 ± 3.70*^{a}	179.40 ± 12.90*^{bc}	207.50 ± 18.60^{b}	157.70 ± 11.40^{c}
	Left	103.10 ± 10.90*^{a}	114.60 ± 9.00*^{a}	210.50 ± 7.00^{b}	169.60 ± 15.90^{c}
Perineurium thickness (µm)	Right	12.30 ± 1.10*^{a}	15.10 ± 2.00*^{a}	13.60 ± 3.90^{a}	25.70 ± 2.10*^{b}
	Left	25.30 ± 2.60*^{a}	24.00 ± 2.00*^{a}	14.70 ± 2.30^{b}	34.30 ± 1.10*^{c}
Endoneurium thickness (µm)	Right	0.30 ± 0.00^{a}	0.30 ± 0.10*^{a}	0.30 ± 0.00^{a}	0.30 ± 0.00*^{a}
	Left	0.30 ± 0.00^{a}	0.60 ± 0.00*^{b}	0.40 ± 0.00^{c}	0.60 ± 0.00*^{b}
Nerve bundle diameter (µm)	Right	379.20 ± 22.10^{a}	532.60 ± 71.90^{b}	576.40 ± 191.50^{b}	797.70 ± 121.10^{c}
	Left	354.90 ± 56.70^{a}	515.10 ± 77.90^{b}	710.90 ± 112.30^{c}	724.90 ± 109.40^{c}
Myelinated nerve fibers diameter (µm)	Right	8.10 ± 1.10*^{a}	6.00 ± 2.70*^{a}	7.70 ± 1.90^{a}	8.30 ± 1.20^{a}
	Left	5.80 ± 1.70*^{a}	11.40 ± 2.10*^{b}	7.70 ± 0.90^{a}	8.20 ± 1.50^{ab}
Myelin sheath thickness (µm)	Right	2.40 ± 0.10*^{a}	3.10 ± 0.20^{b}	3.70 ± 0.20*^{c}	3.80 ± 0.20*^{c}
	Left	3.10 ± 0.10*^{a}	3.00 ± 0.10^{a}	4.90 ± 0.10*^{b}	5.30 ± 1.00*^{b}
Myelinated axon diameter (µm)	Right	3.30 ± 0.70^{a}	2.00 ± 0.10*^{b}	2.60 ± 0.20^{a}	2.80 ± 0.10^{a}
	Left	3.10 ± 0.40^{a}	2.80 ± 0.20*^{a}	3.00 ± 0.20^{a}	2.90 ± 0.10^{a}
Density of myelinated axons per mm²	Right	14,700 ± 765^{a}	24,000 ± 132^{b}	13,000 ± 776*^{c}	18,800 ± 457*^{d}
	Left	14,300 ± 546^{a}	23,600 ± 623^{b}	15,600 ± 156*^{c}	17,300 ± 343*^{d}
Distance between nodes of Ranvier (µm)	Right	56.30 ± 21.10^{a}	47.80 ± 11.60^{a}	76.90 ± 23.30^{ab}	96.10 ± 11.00^{b}
	Left	56.70 ± 17.70^{a}	77.70 ± 22.90^{ab}	70.40 ± 16.60^{ab}	94.30 ± 18.90^{b}

*Asterisk shows significant differences between the right and left sciatic nerves in each parameter ($p < 0.05$).

^{abcd} Different letters show statistical significant differences between the different ages in right or left sciatic nerves in each row ($p < 0.05$).

The maximum nerve fibers diameter of the right and left sciatic nerves was observed at the age of the 40 and 14, respectively. The diameter of myelinated nerve fibers was increasing with chicken growth. The minimum myelin thickness was observed at the age of seven days in the left and right sciatic nerve, respectively. The myelin thickness of the sciatic nerve was increasing in a regular pattern. Maximum and minimum axon diameters were observed at the ages of 7 and 14 days at both sided sciatic nerves. A slow but not regular decrease of axon thickness was observed during the chicken growth.

The change in the average number of myelinated axons per mm^2 (density) in the right and left sciatic nerves did not show a regular pattern. A regular increase in distance between nodes of Ranvier was observed in the right sciatic nerve from the age of 14 days to the age of 40 days.

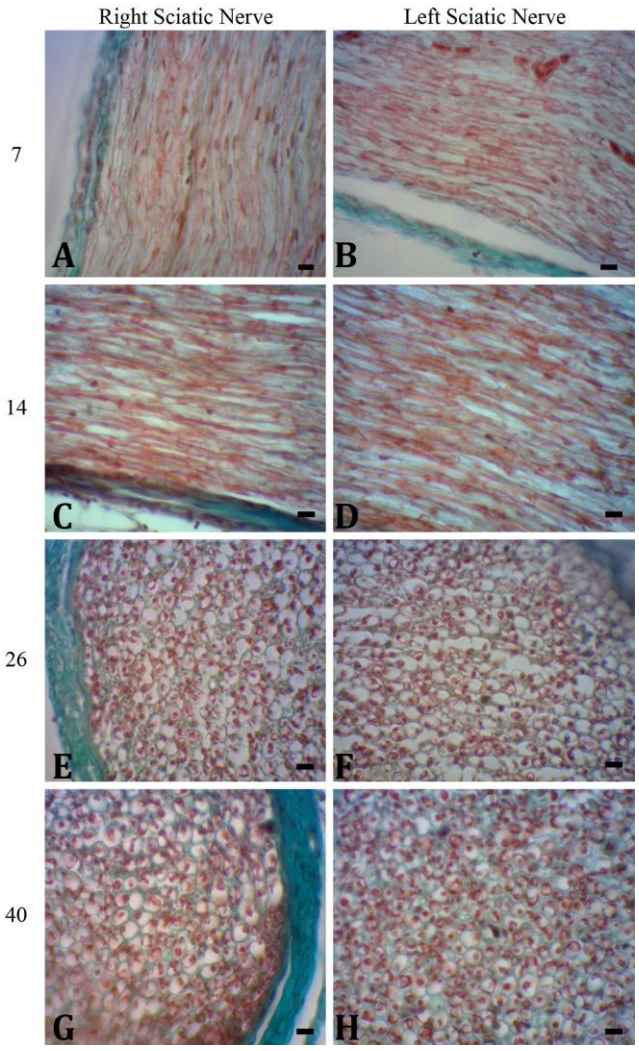

Fig. 2. Histomicrograph of right and left sciatic nerves at the ages of 7, 14, 26 and 40 days old of chicken. **A-D)** Axon, myelin sheath and endoneurium of chickens, **E-H)** Epineurium and nerve bundle of sciatic nerve of chicken, (Masson's trichrome staining; Scale bars = 200 µm).

The increase in distance between nodes of Ranvier in the left sciatic nerve did not have a regular pattern. Figure 2 shows histomicrograph of right and left sciatic nerve at the ages of 7, 14, 26 and 40 days old of chicken.

A compact population of sciatic nerve cell nuclei was identified by the FACT protocol (Fig. 3). The applied FACT protocol resulted in the transparency of the chicken sciatic nerve samples (Fig. 3). Transparency was achieved within 3 days. Furthermore, nuclei were clearly visible in the ~200 µm thickness of the processed tissue (Fig. 3).

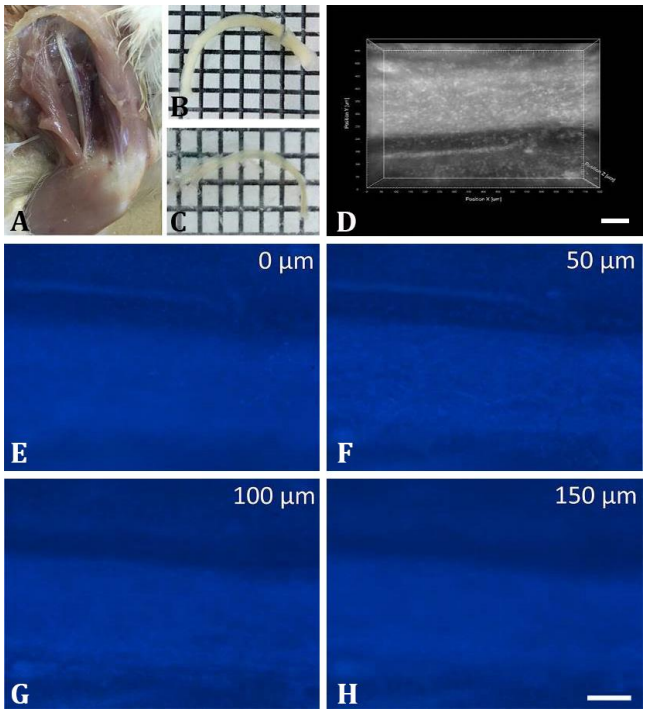

Fig. 3. Whole sciatic nerve clearing and imaging of chicken sciatic nerve using fast free of acrylamide clearing tissue (FACT). **A)** Gross appearance of sciatic nerve in a 26-day-old chicken, **B)** Sciatic nerve before clearing with FACT method (squares are 3.00×3.00 mm), **C)** The same sciatic nerve on day 3 of clearing, **D)** Three-dimensional imaging of sciatic nerve after imaging of 1.00 mm-thickness slices were immunolabelled to detect cells' nuclei with the Hoechst 33342 (Scale bar = 100 µm), **E-H)** Different depths of chicken sciatic nerve after clearing and imaging of tissue using FACT. The cells' nuclei were stained with Hoechst 33342 (Scale bar = 100 µm).

Discussion

Histomorphometry of the sciatic nerve showed that the epineurium, perineurium and endoneurium thickness of the left sciatic nerve was bigger than that of the right sciatic nerve in all age categories of the studied chicken. This was similar to the findings on the sciatic nerve of the rat.[18] The difference in epineurium, perineurium and endoneurium thickness suggested that the left sciatic nerve had more connective tissue than the right in all four chicken age categories. It was presumed that the

epineurium gave strength to the sciatic nerve while the perineurium around the nerve bundle ensured the nerve bundle strength and the endoneurium provide nerve fiber strength. Consisting with our findings, differences were reported in the sciatic nerve of left/right leg in rat and the cat.[19] These variations could call into question the validity and accuracy of using the contralateral nerve as a control in the studies in mammals or birds.

The nerve bundle diameter of the left sciatic in chicken at the age of 26 days was bigger than the right. These findings corresponded to the study on male and female dogs.[20] The difference between the nerve fibers diameter at the ages of 26 and 40 days was not significant. However, the sciatic nerve diameter at the age of 14 days in the left side was more than the right and at the age of seven days in the right side was more than the left side.

The axon diameter and the myelin sheath thickness were bigger in the left sciatic nerve than in the right in all ages' categories except at age of seven days. In contrary the nerve fiber diameter, axon diameter and myelin sheath thickness were bigger in the right sciatic nerve of male and female dogs.[20] Increase in nerve fiber diameter, axon diameter and myelin thickness indicated the sciatic nerve activity.[14]

The distance between nodes of Ranvier was the smallest in chicken of the age of seven days, however, it was the biggest at the age of 40 days. The average distance between nodes of Ranvier at the age of 14 days in the right sciatic nerve was bigger than in the left. Already it was noted that by increasing the diameter of the nerve fibers the speed of transmission of messages and activities were increased.[21] Nodes of Ranvier act as jump places for the exchange and transmission of nerve impulses. Moreover, if the distance between nodes of Ranvier is higher in the nerve fiber, the impulses pass much faster. It can be speculated that the impulse transition rate increases with the age in broiler chickens.

The number of myelinated axons in 1.00 mm^2 (i.e. the density) of the left and right sciatic nerve was the highest at the age of 14 days and the minimum density was at the age of 26 days. The myelinated axon density was higher in the right than in the left sciatic nerve in all age categories except in the 26 days aged chicken. This was opposite to the finding in rabbits in which the number of myelinated nerve fibers was higher in the left than in the right sciatic nerve in both genders.[22]

Dolapchieva *et al.* used the automatic image analysis of the postnatal growth of axons and myelin sheaths in the tibial and perineal nerves of the rabbit and reported that from birth to adulthood the mean axon diameter were increased in both nerves by about 270.00% and the specific width of the myelin sheaths by about 280.00%.[23] Comparing with their findings, in our study, the mean myelinated axon diameter did not change in both the left and right nerves, however, the specific width of the myelin sheaths was increased about 158.30% and 171.00% in the right and left sciatic nerves, respectively. This difference in the growth pattern of axon diameter might be related to the difference growth rate of rabbit and chicken from birth to adulthood. In addition, our samples were collected before adulthood.

Increased speed of nerve impulse transmission occurs because of the increased diameter of the nerve fibers, the distance between the nodes of Ranvier and increased density of nerve fibers (axons).[24] Pannese evaluated morphological changes in nerve cells during aging and found that axons were decreased in number and their myelin sheaths were less compact and undergone segmental demyelination followed by re-myelination.[25]

The FACT protocol for the effective clearing and imaging of immunostained tissues was applied for the first time, on a bird species in our study. For this purpose, we processed the sciatic nerve of the chicken (*Gallus domesticus*). Furthermore, we used Hoechst for nuclei labeling and developed a protocol for this staining type. However, we observed that using glycerol for 12 hr did not solve Hoechst in comparison with FocusClear which was not compatible with DAPI nucleus staining in CLARITY.[2]

The most important result of the tissue clearing is the possibility for optical sectioning used in 3D imaging based on images made with the laser confocal microscope. The availability of this expensive microscope is a big challenge for adapting the tissue imaging for a traditional laboratory. Therefore, we used a Z-stacked motorized stage fluorescent microscope for the imaging of the immuno-labelled tissues. However, this approach has some limitations including the low working distance of available lens of the fluorescent microscope in comparison with the confocal microscope. This discrepancy can be solved by cutting the cleared tissue into 1.00 to 2.00 mm pieces for imaging. Furthermore, the lower penetration of the fluorescent light in comparison with the laser caused limitation of tissue imaging. For that reason, the maximum tissue depth of 150 to 200 μm was reached.

The clearing of the chicken sciatic nerve with FACT protocol required 3 days for completion which was comparable to non-lipid clearing methods such as CUBIC[26] and ScaleA2 and ScaleU2.[27] In addition, removing hydrogel in the FACT protocol needed lower clearing and immunolabelling times than hydrogel-based methods such as CLARITY,[2] PACT,[4] PARS,[4] and SWITCH.[5]

Using the lipid clearing protocols, various types of tissues have been cleared during the recent years in mouse, rat and human. They include brain,[28] spinal cord,[29] lung,[30] heart,[31] liver,[32] kidney,[33] intestine,[34] pancreas,[35] spleen,[36] mammary gland,[37] ovary,[38] skeletal muscle,[39] bone,[40] eye,[41] and skin.[42] There is article study that used FACT for clearing mouse and rat tissues.[43] However, our study was the first record that cleared sciatic nerve in chicken using the FACT protocol.

In conclusion, histomorphometric parameters in the left and right sciatic nerves during chicken growth were not symmetrically. Furthermore, the FACT protocol was a simple technique and could be appropriate for the use in laboratories in developing countries that lack advanced microscopes such as confocal microscope. The FACT protocol could be used for 3D imaging of the sciatic nerve and its immuno-stained evaluation.

Acknowledgments

This research was financially supported by the Vice Chancellor for Research of the School of Veterinary Medicine, Shiraz University.

Conflict of interest

There is no conflict of interest to declare.

References

1. Dodt H-U, Leischner U, Schierloh A, et al. Ultramicroscopy: three-dimensional visualization of neuronal networks in the whole mouse brain. Nat Methods 2007; 4(4):331-336.
2. Tomer R, Ye L, Hsueh B, et al. Advanced CLARITY for rapid and high-resolution imaging of intact tissues. Nat Protoc 2014; 9(7):1682-1697.
3. Chung K, Wallace J, Kim SY, et al. Structural and molecular interrogation of intact biological systems. Nature 2013; 497(7449):332-337.
4. Yang B, Treweek JB, Kulkarni RP, et al. Single-cell phenotyping within transparent intact tissue through whole-body clearing. Cell 2014; 158(4):945-958.
5. Murray E, Cho JH, Goodwin D, et al. Simple, scalable proteomic imaging for high-dimensional profiling of intact systems. Cell 2015; 163(6):1500-1514.
6. Liu AKL, Lai HM, Chang RC-C, et al. Free of acrylamide sodium dodecyl sulphate (SDS)-based tissue clearing (FASTClear): a novel protocol of tissue clearing for three-dimensional visualization of human brain tissues. Neuropathol Appl Neurobiol 2017;43(4): 346-351.
7. Xu N, Tamadon A, Liu Y, et al. Fast free-of-acrylamide clearing tissue (FACT)- an optimized new protocol for rapid, high-resolution imaging of three-dimensional brain tissue. Scientific Reports 2017; 7(1):9895. doi:10.1038/s41598-017-10204-5.
8. Oliveira FS, Nessler RA, Castania JA, et al. Ultra-structural and morphometric alterations in the aortic depressor nerve of rats due to long term experimental diabetes: effects of insulin treatment. Brain Res. 2013; 1491:197-203.
9. Sanada LS, Tavares MR, Neubern MCM, et al. Can Wistar rats be used as the normotensive controls for nerve morphometry investigations in spontaneously hypertensive rats (SHR)? Acta Cir Bras 2011; 26(6):514-520.
10. Dolapchieva S. Computer-assisted morphometric study on the postnatal growth of axon size and myelin thickness in the ventral and dorsal roots of the rabbit. Ann Anat 2004; 186(1):61-68.
11. Ronchi G, Jager SB, Vaegter CB, et al. Discrepancies in quantitative assessment of normal and regenerated peripheral nerve fibers between light and electron microscopy. J Peripher Nerv Syst 2014; 19(3):224-233.
12. Barreiros VCP, Dias FJ, Iyomasa MM, et al. Morphological and morphometric analyses of crushed sciatic nerves after application of a purified protein from natural latex and hyaluronic acid hydrogel. Growth Factors 2014; 32(5):164-170.
13. Kemp J, Després O, Pebayle T, et al. Differences in age-related effects on myelinated and unmyelinated peripheral fibres: a sensitivity and evoked potentials study. Eur J Pain 2014; 18(4):482-488.
14. Ikeda M, Oka Y. The relationship between nerve conduction velocity and fiber morphology during peripheral nerve regeneration. Brain Beha 2012; 2(4):382-390.
15. Fischer AH, Jacobson KA, Rose J, et al. Hematoxylin and eosin staining of tissue and cell sections. CSH Protoc 2008; 2008:pdb.prot4986. doi: 10.1101/pdb.prot4986.
16. Foot NC. The Masson trichrome staining methods in routine laboratory use. Stain Technol 1933; 8(3): 101-110.
17. Mohammad Rezazadeh F, Saedi S, Rahmanifar F, et al. Fast free of acrylamide clearing tissue (FACT) for clearing, immunolabelling and three-dimensional imaging of partridge tissues. Microsc Res Tech 2018; 81(12):1374-1382.
18. Sta M, Cappaert NLM, Ramekers D, et al. The functional and morphological characteristics of sciatic nerve degeneration and regeneration after crush injury in rats. J Neurosci Methods 2014; 222:189-198.
19. Christensen MB, Tresco PA. Differences exist in the left and right sciatic nerves of naïve rats and cats. Anat Rec (Hoboken). 2015; 298(8):1492-1501.
20. Vujaskovic Z, Gillette SM, Powers BE, et al. Effects of intraoperative hyperthermia on canine sciatic nerve: histopathologic and morphometric studies. Int J Hyperthermia 1994; 10(6):845-855.
21. Perge JA, Niven JE, Mugnaini E, et al. Why do axons differ in caliber? J Neurosci. 2012; 32(2):626-638.
22. Muglia U, Vita G, Laura R, et al. Morphometric comparison between contralateral sciatic nerves in the male and female rabbit. Anat Histol Embryol 1997; 26(2):147-150.
23. Dolapchieva S, Eggers R, Kühnel W. Automatic image analysis of the postnatal growth of axons and myelin sheaths in the tibial and peroneal nerves of the rabbit. Ann Anat 2000; 182(2):133-142.

24. Hartline DK, Colman DR. Rapid conduction and the evolution of giant axons and myelinated fibers. Curr Biol 2007; 17(1):R29-35.
25. Pannese E. Morphological changes in nerve cells during normal aging. Brain Struct Funct. 2011; 216(2):85-89.
26. Susaki EA, Tainaka K, Perrin D, et al. Whole-brain imaging with single-cell resolution using chemical cocktails and computational analysis. Cell 2014; 157(3):726-739.
27. Hama H, Kurokawa H, Kawano H, et al. Scale: a chemical approach for fluorescence imaging and reconstruction of transparent mouse brain. Nat Neurosci 2011; 14(11):1481-1488.
28. Zheng H, Rinaman L. Simplified CLARITY for visualizing immunofluorescence labeling in the developing rat brain. Brain Struct Funct 2016; 221(4): 2375-2383.
29. Liang H, Schofield E, Paxinos G. Imaging serotonergic fibers in the mouse spinal cord using the CLARITY/CUBIC technique. J Vis Exp 2016(108): 53673. doi: 10.3791/53673
30. Saboor F, Reckmann AN, Tomczyk CUM, et al. Nestin-expressing vascular wall cells drive development of pulmonary hypertension. Eur Respir J 2016; 47(3): 876-888.
31. Ding Y, Lee J, Ma J, et al. Light-sheet fluorescence imaging to localize cardiac lineage and protein distribution. Sci Rep 2017; 7:42209. doi: 10.1038/ srep42209.
32. Font-Burgada J, Shalapour S, Ramaswamy S, et al. Hybrid periportal hepatocytes regenerate the injured liver without giving rise to cancer. Cell 2015; 162(4): 766-779.
33. Unnersjö-Jess D, Scott L, Blom H, et al. Super-resolution stimulated emission depletion imaging of slit diaphragm proteins in optically cleared kidney tissue. Kidney Int 2016; 89(1):243-247.
34. Neckel PH, Mattheus U, Hirt B, et al. Large-scale tissue clearing (PACT): Technical evaluation and new perspectives in immunofluorescence, histology, and ultrastructure. Sci Rep 2016; 6:34331. doi: 10.1038/ srep34331.
35. Muzumdar MD, Dorans KJ, Chung KM, et al. Clonal dynamics following p53 loss of heterozygosity in Kras-driven cancers. Nat Commun 2016; 7:12685. doi: 10.1038/ncomms12685.
36. Murray K, Godinez DR, Brust-Mascher I, et al. Neuroanatomy of the spleen: Mapping the relationship between sympathetic neurons and lymphocytes. PLoS One 2017; 12(7):e0182416. doi: 10.1371/journal. pone.0182416.
37. Lloyd-Lewis B, Davis FM, Harris OB, et al. Imaging the mammary gland and mammary tumours in 3D: optical tissue clearing and immunofluorescence methods. Breast Cancer Res 2016; 18(1):127. doi: 10.1186/ s13058-016-0754-9.
38. Hu W, Tamadon A, Hsueh AJW, et al. Three-dimensional reconstruction of the vascular architecture of the passive CLARITY-cleared mouse ovary. J Vis Exp 2017(130):56141. doi: 10.3791/56141.
39. Zhang WL, Liu SH, Zhang WC, et al. Skeletal muscle CLARITY: A preliminary study of imaging the three-dimensional architecture of blood vessels and neurons. Cell J 2018; 20(2):132-137.
40. Greenbaum A, Chan KY, Dobreva T, et al. Bone CLARITY: Clearing, imaging, and computational analysis of osteoprogenitors within intact bone marrow. Sci Transl Med 2017; 9(387): 6518. doi: 10.1126/scitranslmed.aah6518.
41. Singh JN, Nowlin TM, Seedorf GJ, et al. Quantifying three-dimensional rodent retina vascular development using optical tissue clearing and light-sheet microscopy. J Biomed Opt 2017; 22(7): 76011. doi: 10.1117/1.JBO.22.7.076011.
42. Lisovsky A, Zhang DKY, Sefton MV. Effect of methacrylic acid beads on the sonic hedgehog signaling pathway and macrophage polarization in a subcutaneous injection mouse model. Biomaterials. 2016; 98:203-214.
43. Khoradmehr A, Mazaheri F, Anvari M, et al. A simple technique for three-dimensional imaging and segmentation of brain vasculature using fast free-of-acrylamide clearing tissue in murine. Cell J 2019; 21(1):49-56.